International Journal of Optomechatronics
Publication details, including instructions for authors and subscription information:
http://www.tandfonline.com/loi/uopt20

A Vision-Based Methodology to Dynamically Track and Describe Cell Deformation during Cell Micromanipulation

Fatemeh Karimirad [a], Bijan Shirinzadeh [a], Wenyi Yan [b] & Sergej Fatikow [c]

[a] Robotics and Mechatronics Research Laboratory, Monash University, Melbourne, Australia

[b] Department of Mechanical and Aerospace Engineering, Monash University, Melbourne, Australia

[c] Department of Computing Science, University of Oldenburg, Oldenburg, Germany

Version of record first published: 13 Feb 2013.

To cite this article: Fatemeh Karimirad , Bijan Shirinzadeh , Wenyi Yan & Sergej Fatikow (2013): A Vision-Based Methodology to Dynamically Track and Describe Cell Deformation during Cell Micromanipulation, International Journal of Optomechatronics, 7:1, 33-45

To link to this article: http://dx.doi.org/10.1080/15599612.2012.744433

International Journal of Optomechatronics, 7: 33–45, 2013

ISSN: 1559-9612 print/1559-9620 online
DOI: 10.1080/15599612.2012.744433

Taylor & Francis
Taylor & Francis Group

A VISION-BASED METHODOLOGY TO DYNAMICALLY TRACK AND DESCRIBE CELL DEFORMATION DURING CELL MICROMANIPULATION

Fatemeh Karimirad,[1] Bijan Shirinzadeh,[1] Wenyi Yan,[2] and Sergej Fatikow[3]

[1]*Robotics and Mechatronics Research Laboratory, Monash University, Melbourne, Australia*

[2]*Department of Mechanical and Aerospace Engineering, Monash University, Melbourne, Australia*

[3]*Department of Computing Science, University of Oldenburg, Oldenburg, Germany*

The main objective of this article is to mechanize the procedure of tracking and describing the various phases of deformation of a biological circular cell during micromanipulation. The devised vision-based methodology provides a real-time strategy to track and describe the cell deformation by extracting a geometric feature called dimple angle. An algorithm based on Snake was established to acquire the boundary of the indenting cell and measure the aforementioned feature. Micromanipulation experiments were conducted for zebrafish embryos. Experimental results were used to characterize the deformation of the manipulating embryo by the devised geometric parameter. The results demonstrated the high capability of the methodology. The proposed method is applicable to the micromanipulation of other circular biological embryos such as injection of the mouse oocytelembryo. Supplemental materials are available for this article. Go to the publisher's online edition of the International Journal of Optomechatronics to view the supplemental files.

Keywords: contour extraction, image processing, image segmentation, microrobotic cell injection

1. INTRODUCTION

Micro/nano positioning and manipulation mechanisms and systems play important roles in science and engineering applications such as scanning tunnel microscopy, atomic force microscopy, X-ray lithography, bio-medicine, cell surgery and nano surgery, and micro/nano surface metrology and characterization (Liaw, Shirinzadeh, and Smith 2009; Zubir, Shirinzadeh, and Tian 2009). Manipulation of biological specimens such as cell injection is one of the important applications of such micromanipulation methodologies and systems. The limitations of the conventional manual cell injection such as low success rates, long training requirement,

Address correspondence to Fatemeh Karimirad, Robotics and Mechatronics Research Laboratory, Monash University, Building 37 (Wellington Road), Clayton, Victoria 3800, Australia. E-mail: Fatemeh.Karimirad@monash.edu

NOMENCLATURE

α	dimple angle, degree	R	2-D array containing the results of the pattern matching procedure
d	displacement of the micropipette, μm	T	2-D array containing the intensities values of the template of interest pixels
H	height of the current frame, pixel	W	width of the current frame, pixel
H'	height of the template of interest, pixel	W'	width of the template of interest, pixel
I	2-D array containing the intensities values of the current frame pixels		
r	radius of the embryo, μm		

contamination and poor reproducibility require the reduction of direct human involvement in the biological cell injection process. One aspect of the development of an automated vision-based cell injection is the extraction of the geometric features of the deformed cell during the injection process. These data have been used to propose a theoretical model to study and characterize the mechanical properties of biological cells, and to find the relationship between the deformation of a cell and the associated force (Sun et al. 2003; Tan et al. 2008). There have been many research efforts and developments directed toward automation of microinjection (Li, Zong, and Bi 2001; Kumar, Kapoor, and Taylor 2003; Matsuoka et al. 2005; Mattos et al. 2007; Wang, Liu, and Sun 2009; Huang et al. 2009; Wang et al. 2007; Yu and Nelson 2001; Ammi and Ferreira 2006). However relatively few research efforts have addressed the aforementioned issue. Sun et al. characterized the membrane shape of a cell with three parameters: the radius of the semicircular curved surface and the radius and depth of the indentation created by the micromanipulator (Sun et al. 2003). They calculated the Young's Modulus of mouse oocyte using their proposed point-load model. They extracted the required properties manually from the images of the injection process. Tan et al. derived differential equations from the equilibrium equation in the contact and noncontact regions (Tan et al. 2008). In order to solve these equations, a complex numerical computation procedure is required. Lu et al. represented the concavity of the parabola to model the indentation area of the deformed cell membrane (Lu et al. 2009). They recorded and processed off-line cell deformation images to measure the cell boundary. Han et al. also used a parabola model as well as an ellipse model to describe changes of membranes strain (Han et al. 2011). Diaz et al. tracked various phases of mouse oocyte deformation to mechanize the deployment of rotational oscillations of the micropipette during injection (Diaz et al. 2010). They defined the membrane profile by a two-dimensional surface function in the meridian plane. They developed a routine to trace the oolemma profile, although this routine requires a starting point selected manually. A possible limitation with the above methods is that most of these do not function in real-time. These methods record and process cell deformation images in off-line mode; otherwise, they take the displacement of the micropipette as the deformation of the cell. In this article, we introduce a novel idea to describe the indentation of a circular cell in real-time. Using this method, deformation of the injecting cell is quantified in real-time using well-established image processing algorithms without the need to develop complex mathematics. A robust deformable cell boundary detection algorithm based on Snake (Kass, Witkin, and Terzopoulos 1988) is utilized to effectively track the deformation of the cell during the injection process.

The boundary detection algorithm used in the proposed method is similar to the procedure Ammi et al. used in their paper for detecting the boundary of the injecting cell (Ammi and Ferreira 2006). However, some additional preprocessing steps have been performed to improve the accuracy and efficiency of their algorithm. The proposed scheme enables the biologist to characterize an individual cell behavior at different indentations. This article is organized as follows. Section 2 presents the methodology which consists of the techniques for image enhancement, micropipette localization, boundary detection and cell shape description. Section 3 provides the experimental setup and the results. Finally section 4 is the conclusion and the future work.

2. METHODOLOGY

The components of a microrobotic cell injection system for a suspended cell are shown in Figure 1. These include two micromanipulators for precise positioning of the microcapillaries, two microinjectors, one for injection mechanism and the other for suction mechanism and two microcapillaries, one for a precise delivery of a compound into the cell and the other for holding the cell, as well as a vision system for visualization consisting of an optical microscope, a camera connected to a workstation, and a software developed for image processing. Successful autonomous injection needs robust algorithms for image segmentation and visual tracking of the cell. The speed of vision systems strongly depends on the speed of localization and recognition procedures. A typical image of a cell micromanipulation scene is depicted in Figure 2. The presence of some undesirable objects such as image noise makes the direct use of tracking algorithm impossible. Thus some pre-processing steps were required to mask these objects. The position of the injection micropipette was also required in order to find the position of the contact point. Detection of injection micropipette was considered as a pattern matching problem. Morphological operations and feature detection algorithm were utilised to enhance the image

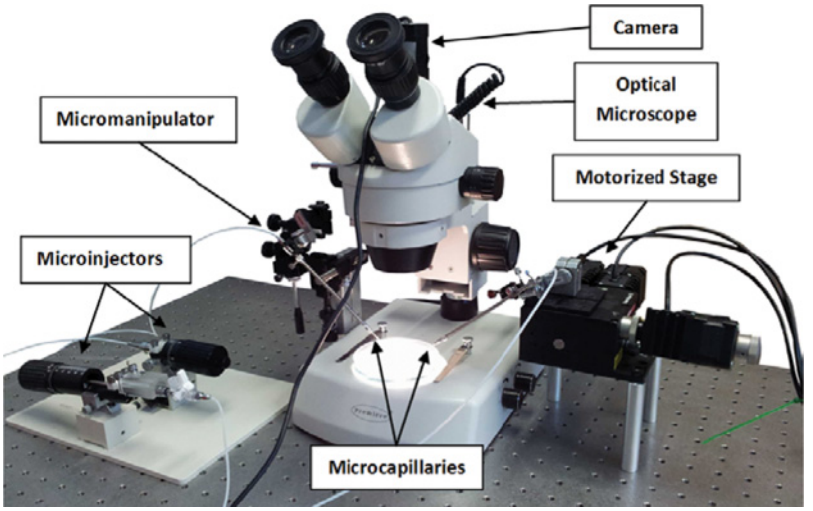

Figure 1. Automated bio-micromanipulation system (color figure available online).

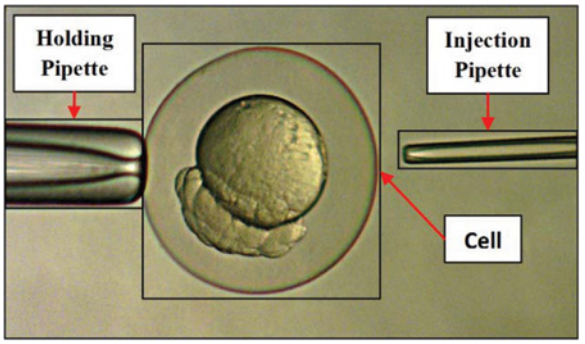

Figure 2. A typical image of a cell micromanipulation (color figure available online).

and remove the undesirable objects within image to provide for a more robust and faster tracking. The overall procedure of the method is shown in Figure 3, with the step by step function of the processes and methodology.

2.1. Pipette Detection Procedure

Pipette detection algorithm was initiated for injection micropipette using a template matching algorithm. The template of the interest is given as the input to the template matching algorithm. The matching procedure scans through the original image, and compares overlapped patches with the template using the specified method and stores the comparison results. Following the completion of the comparison process, the best match can be found. Normalized sum of squared difference (SSD) was used as the method of matching in the developed methodology since it is simple, flexible, and robust for this application. The injection micropipette is small and does not present many edge features. Consequently, the use of all template pixels instead of just the edge pixels improves the robustness of the matching algorithm (Mattos et al. 2009). The normalized SSD correlation algorithm is described by the following relationship:

$$R(x,y) = \frac{\sum_{x',y'} [T(x',y') - I(x+x',y+y')]^2}{\sqrt{[\sum_{x',y'} T(x',y')^2 \cdot \sum_{x',y'} I(x+x',y+y')^2]}} \tag{1}$$

where

$$0 \le x' \le w' - 1,$$
$$0 \le y' \le h' - 1,$$

and I, T and R denote the current frame, template, and the result respectively. The sum is over $x'y'$ under the window containing the feature positioned at x, y. w and h are width and height of the current frame and w' and h' are width and height of the template. A close-up image of the injection micropipette was defined as the template

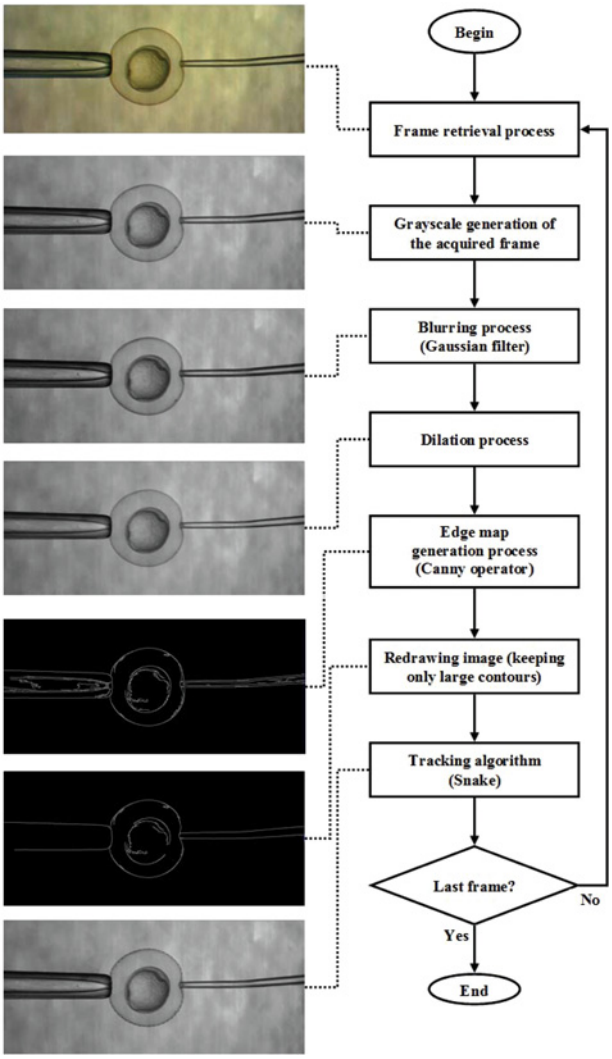

Figure 3. Flowchart of the cell boundary detection procedure (color figure available online).

of interest. It was assumed that the cell is held via the holding micropipette from the left side and the injecting pipette was located in the right side of the image. Thus the pattern matching algorithm searched just the right side of the image for the injection micropipette as shown in the following:

$$(w-1)/2 \leq x \leq w-1$$
$$0 \leq y \leq h-1.$$

One problem we had with this method in our application was that when the injection micropipette contacted the cell and started piercing the cell, the template did not

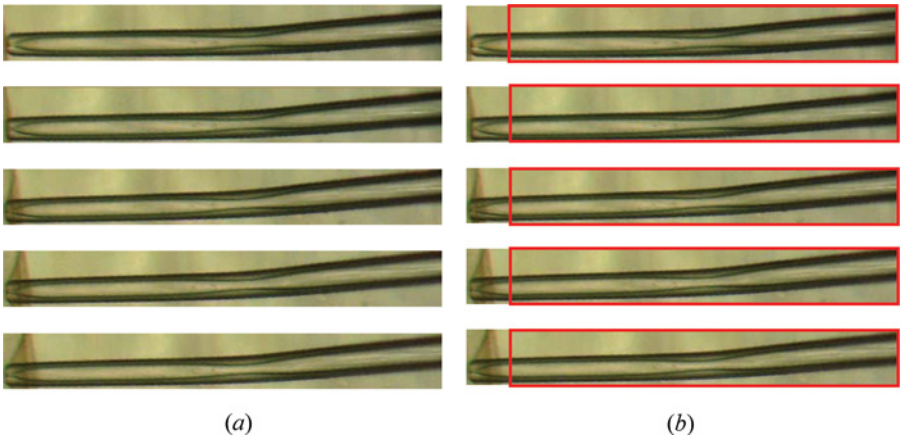

Figure 4. Injection micropipette template changes (*a*) while the last part of it is fixed (*b*) during injection process (color figure available online).

match the injection micropipette any more. Figure 4*a* shows how the injection micropipette template changed during the injection process. To overcome this problem the initial template was trimmed only to cover the last part of the injection micropipette which was unchanged during injection process as depicted in Figure 4*b*. Taking this offset into account, the position of the tip of the injection micropipette may be achieved.

2.2. Image Enhancement Procedure

The non-uniform illumination in the background of the cell injection scene disturbed tracking algorithm. In order to remove undesirable components such as image noise, image enhancement procedure was applied. The first step was the segmentation of the binarized image and breaking it into several non-overlapped contours. The objects in the cell injection process were too close together and the contour finder algorithm recognized the cell and the pipettes as one object. Thus, prior to finding counters, some morphological filters were required to be applied to expand the distances between objects, and compensate for the disjoints within objects boundaries. After finding contours, the image may be redrawn by keeping only the contours larger than a specified threshold.

2.3. Tracking Algorithm Development

A robust adaptive algorithm was required to detect the cell boundary and track it in the subsequent frames. There have been many studies in the area of contour extraction, and a number of methods have been developed. The gradient-based Prewitt, Sobel and Laplace detector (Davis 1975) uses edge detection operators. There are also other methods, such as second derivative zero-crossing detector (Marr and Hildreth 1980) or computational scheme based on the Canny criteria (Canny 1986). These methods frequently fail due to their inability to deal with noise and

non-uniform illumination. Thus, all of the above methods usually require some post-processing steps. Kass et al. proposed a new approach towards image segmentation called Active Contour (Kass, Witkin, and Terzopoulos 1988). An Active Contour or Snake is a dynamically evolving curve that gets attracted towards the object edges while trying to minimize its energy. Since Snake does not only depend on the intensity but also the curvature and continuity of the boundary pixels, it is less sensitive to the noise. After the image enhancement procedure was performed, Snake may be applied to provide active contouring.

2.4. Cell Shape Description

The polygon of control points obtained by Snake approximates the cell boundary but in order to characterize the mechanical behavior of membrane deformation, a geometric parameter is required. When a micropipette exerts a uniaxial indentation force to a circular embryo, a dimple is created around the contact point. If the contact point is connected to its successive control point in the right half and the symmetric point in the left half of the embryo, an angle is revealed. The contact point is the vertex of the angle and the connecting lines from the vertex to the right and left adjacent points are the sides of the angle. The aforementioned angle is referred to as the dimple angle in the rest of the paper. An example of a dimple angle is illustrated in Figure 5. Having the coordinates of the control points obtained by Snake as well as the injection micropipette location acquired by the pattern matching algorithm, the magnitude of this angle can be estimated. In practice, the dimple angle is the sum of the angles of the tangencies at both right and left sides of the micropipette edge. The angle of tangency with the outside of the micropipette is extrapolated from the control points adjacent to the outside of the micropipette. The dimple angle is utilized to characterize the indented embryo in the proposed method. The result and discussion of the experimental data for zebrafish embryo will be presented in the next section.

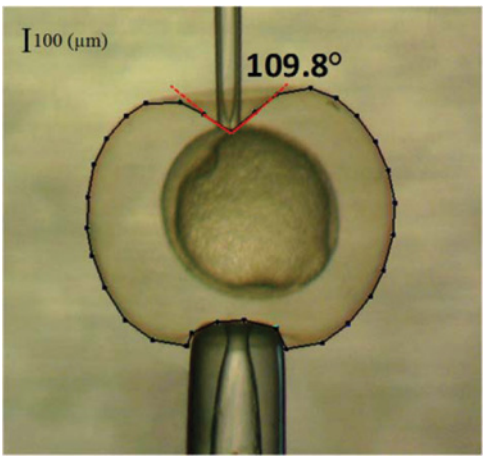

Figure 5. An example illustrating the dimple angle within a deformed cell (color figure available online).

3. EXPERIMENT DESIGN AND RESULTS

3.1. Experimental Setup

A micromanipulation system for indenting zebrafish embryo was developed as shown in Figure 1. The system included a flexure based precision stage (MAX343 of Thorlabs, Inc.) to which the injection micropipette holder was clamped via a precision fixture as shown in the figure. The stage was driven by 3 DC stepper motors producing motion along each Cartesian coordinate that makes it possible to move towards to the target embryo, touch it and deform it. Another micropipette holder was mounted on a joystick micromanipulator (MN-151 of Narishige Inc.) to hold the holding micropipette in order to suck and fix the suspended embryo to be able to inject to it. The platform was attached to a vibration isolation table. The real experiments were conducted at room temperature for several zebrafish embryos. The embryos were at the developmental stage between 4(h) and 6(h) after fertilization. The embryos were kept in a petridish containing E3 Medium during the micromanipulation process. The target embryo was fixed by a holding micropipette 100(μm) in inner diameter and 400(μm) in outer diameter and indented by a micropipette 20(μm) in inner diameter and 100(μm) in outer diameter. The deformation of the embryo and the motion of the motorized stage were captured by a USB camera (Dino-Lite Digital USB Microscope Camera Eyepiece AM423 with 1280×1024 pixel images and maximum of 30 fps with pixels resolution of 4 μm), and the images were transmitted to a computer (Quad Core 2.8 GHz) to be processed. OpenCV package was used for developing the image processing routines.

3.2. Experimental Results

After the preprocessing steps had been performed, the Snake was initiated using the Hough transform (Hough 1959). Hough transform found the best circular approximation of the shape of the un-deformed embryo. The movement and deformation of an embryo were small during the micromanipulation between consecutive frames. Thus, there was no need to initialize Snake in all frames. Instead, the output of the previous frame was used as the initial contour for the next frame. It is depicted in Figure 6 that Snake kept track the deformation of the embryo during the micromanipulation. The coordinates of the contact point which is the tip of the injection micropipette was found with the help of the template matching algorithm. The dimple angle was estimated using the Snake control points as well as the injection micropipette location. In order to increase the accuracy of our calculation, a quadratic interpolation was fitted to the control points within the contact area. The dimple angle was estimated by calculating the tangent lines at the edges of both sides of the micropipette. Figure 7 shows the estimated dimple angle for several zebrafish embryos in the same stage of development during the course of the indentation. It is seen in the figure that the proposed parameter has a descending trend and significant range as the indentation depth increases. Thus, this angle truly satisfies the requirement for characterizing an indented circular embryo. Table 1 shows the mean of the computational time required for each of the image processing steps. The total computational time was reasonable for the real-time micromanipulation.

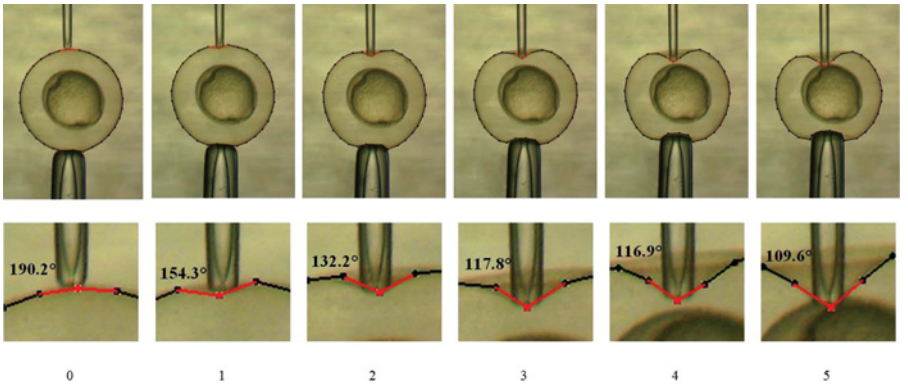

Figure 6. Tracking zebrafish embryo deformation during micromanipulation (color figure available online).

3.3. Regression Analysis

It was observed that the dependency of the dimple angle to the displacement of the micropipette is not linear as depicted in Figure 7. In order to identify possible correlation between the dimple angle and the displacement, a statistical analysis was conducted. The results show that there is a strong relationship ($R2 \approx 95\%$) between the dimple angle and the 2nd order of the displacement of the micropipette. This can be described as a model derived from regression of ln (α) on d as shown in the following:

$$\mathrm{Ln}(\alpha) = 1.573e - 06 * d^2 - 0.00275147 * d + 5.29055 \quad (2)$$

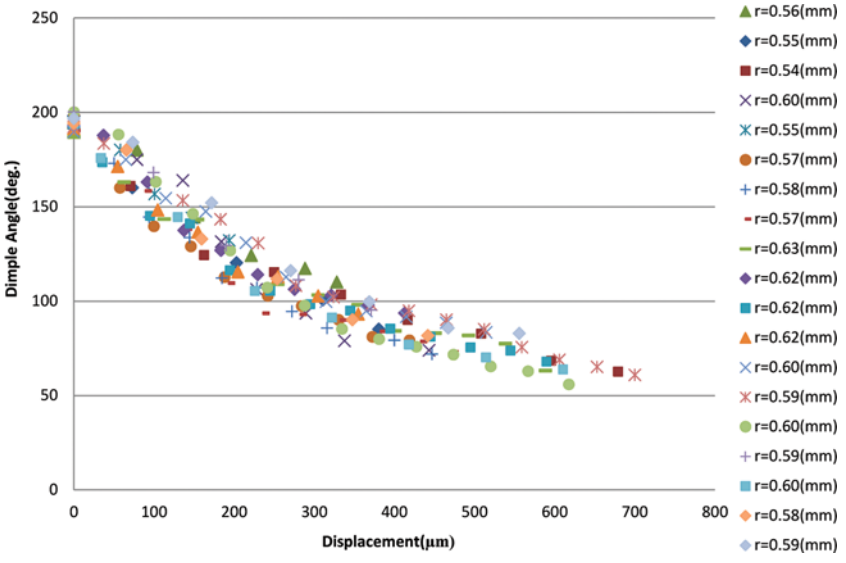

Figure 7. Estimation of dimple angle using interpolation based on the experimental data of indentation of multiple zebrafish embryos (color figure available online).

Table 1. Mean computational times for each of the image processing steps

Image processing steps	Computational time (ms)
Micropipette detection	26.31
Tracking algorithm	28.85
Image enhancement	15.68
Total	70.84

where α is the dimple angle and d is the displacement of the micropipette. The fitted curve is depicted in Figure 8. There is a strong agreement between the output generated by the model and the experimental data as shown in Figure 9. It was also investigated to determine whether or not there is a relationship between the dimple angle and the radius of the embryo. In doing so the following relationship was identified:

$$\ln(\alpha) = 1.56648e - 06 * d^2 - 0.00275409 * d + 0.000564735 * r + 4.95714 \qquad (3)$$

where α is the dimple angle, d is the displacement of the micropipette and r is the radius of the embryo. The resulting parameters of the analysis are summarized in Table 2, and they show that the radius does not significantly improve the model since its inclusion only increases the r^2 by 0.11%. This can further be confirmed in Figure 10 where there is no observable trend in the graph in terms of dependency on the radius. Thus, the contribution of the radius in fact is very small, whereas the displacement alone explains 95% of the variability.

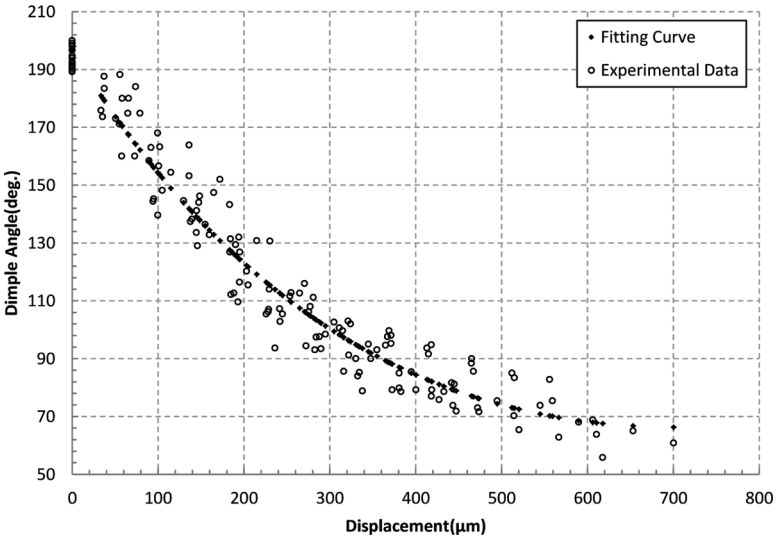

Figure 8. Fitting a curve to the experimental data of zebrafish micromanipulation.

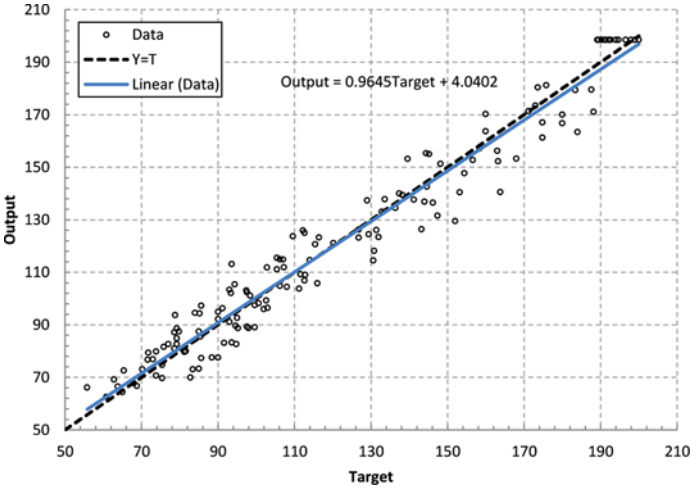

Figure 9. The agreement of the output generated by regression with the experimental data (Target) (color figure available online).

Table 2. Summary of regression analysis (*a*) with and (*b*) without the contribution of radius

Term	Coef.	T	P
(*a*)			
Constant	4.95714	26.1746	0.000
$\mathbf{d^2}$	1.56648e-06	8.1717	0.000
d	−0.00275409	−24.2084	0.000
r	0.000564735	1.7655	0.080
S = 0.0757191	R-Sq = 95.13%	R-Sq(adj) = 95.03%	
(*b*)			
Constant	5.29055000	366.389	0.000
$\mathbf{d^2}$	1.573e-06	8.147	0.000
d	−0.00275147	−24.009	0.000
S = 0.0762814	R-Sq = 95.02%	R-Sq(adj) = 94.95%	

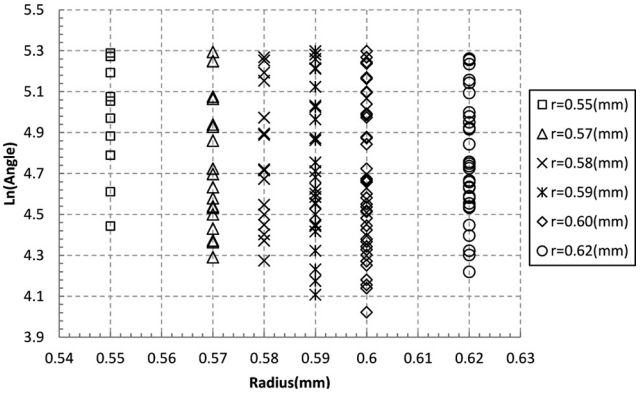

Figure 10. Relationship between the radius of the zebrafish embryos and the natural logarithm of the dimple angle during the course of the indentation.

4. CONCLUSION

A real time vision-based methodology has been proposed and developed to track the deformation of a circular embryo dynamically during micromanipulation. The proposed method captures and processes every frame by image segmentation of the embryo and the injection micropipette. A robust and deformable contour extraction algorithm was established. During micromanipulation, embryo deformation was tracked and the deformation of the embryo was quantified by the proposed geometry feature called dimple angle. Non-linear regression has been performed to relate the devised angle to the displacement of the micropipette and the radius of the embryo. There appears to be no relationship between the dimple angle and the radius but a strong dependency of the dimple angle to the displacement. It is possible that the range of radii of zebrafish embryo may be very small for the effect to show up. The proposed method is applicable to the micromanipulation of other circular biological embryos such as the injection of mouse oocyte/embryo. We hypothesize that the embryo rupturing takes place during injection process in a specific angle for the same kind of cells such as zebrafish embryo at the same developmental stage. We intend to make the study of this hypothesis in our future work.

ACKNOWLEDGMENT

This research is supported by Australian Research Council, ARC Discovery-DP0666366, ARC LIEF-LE0668508, ARC LIEF-LE0347024, and ARC Discovery-DP0986814. The authors also would like to thank Mr. Julian Cocks, the aquarium manager of the ARMI FishCore facility and its staff, and Mr. Alan Couchman, of the School of Mathematical science for proof-reading and assistance in the preparation of this manuscript.

REFERENCES

Ammi, M. and A. Ferreira. 2006. Biological cell injection visual and haptic interface. *Advanced Robotics* 20 (3): 283–304.

Canny, J. 1986. A computational approach to edge detection. *IEEE Transactions on Pattern Analysis and Machine Intelligence* 8: 184–203.

Davis, L. S. 1975. A survey of edge detection techniques. *Computer Graphics and Image Processing* 4 (3): 248–270.

Diaz, J. F., M. Karzar-Jeddi, N. Olgac, T. H. Fan, and A. F. Ergenc. 2010. Geometric characterization of cell membrane of mouse oocytes for ICSI. *Journal of Biomechanical Engineering* 132: 121002.

Han, M. L., Y. L. Zhang, M. Y. Yu, C. Y. Shee, and W. T. Ang. 2011. Real-time modeling and control of the circular cell membranes strain. *IEEE International Conference on Robotics and Animation*, 4115–4120. Shanghai, China.

Hough, P. V. C. 1959. Machine analysis of bubble chamber pictures. *International Conference on High Energy Accelerators and Instrumentation*, 554–556.

Huang, H. B., D. Sun, J. K. Mills, and S. H. Cheng. 2009. Robotic cell injection system with position and force control: Toward automatic batch biomanipulation. *Robotics, IEEE Transactions on* 25 (3): 727–737.

Kass, M., A. Witkin, and D. Terzopoulos. 1988. Snakes: Active contour models. *International Journal of Computer Vision* 1 (4): 321–331.

Kumar, R., A. Kapoor, and R. H. Taylor. 2003. Preliminary experiments in robot/human cooperative microinjection. *IEEE International Conference on Intelligent Kobots and Systems*, 3186–3191. Las Vegas, NV.

Li, X., G. Zong, and S. Bi. 2001. Development of global vision system for biological automatic micro-manipulation system. Paper read at IEEE International Conference on Robotics and Automation (ICRA 2001), at Seoul, Korea.

Liaw, H. C., B. Shirinzadeh, and J. Smith. 2009. Robust neural network motion tracking control of piezoelectric actuation systems for micro/nanomanipulation. *IEEE Transactions on Neural Networks* 20 (2): 356–367.

Lu, Zhe, Peter C. Y. Chen, Hong Luo, Joohoo Nam, Ruowen Ge, and Wei Lin. 2009. Models of maximum stress and strain of zebrafish embryos under indentation. *Journal of Biomechanics* 42 (5): 620–625.

Marr, D. and E. Hildreth. 1980. Theory of edge detection. *Proceedings of the Royal Society of London. Series B, Biological Sciences* 207 (1167): 187–217.

Matsuoka, H., T. Komazaki, Y. Mukai, M. Shibusawa, H. Akane, A. Chaki, N. Uetake, and M. Saito. 2005. High throughput easy microinjection with a single-cell manipulation supporting robot. *Journal of Biotechnology* 116 (2): 185–194.

Mattos, L., E. Grant, R. Thresher, and K. Kluckman. 2007. New developments towards automated blastocyst microinjections. *IEEE International Conference on Robotics and Automation*, 1924–1929. Rome, Italy.

Mattos, L. S., E. Grant, R. Thresher, and K. Kluckman. 2009. Blastocyst microinjection automation. *Information Technology in Biomedicine, IEEE Transactions on* 13 (5): 822–831.

Sun, Y., K. T. Wan, K. P. Roberts, J. C. Bischof, and B. J. Nelson. 2003. Mechanical property characterization of mouse zona pellucida. *NanoBioscience, IEEE Transactions on* 2 (4): 279–286.

Tan, Y., D. Sun, W. Huang, and S. H. Cheng. 2008. Mechanical modeling of biological cells in microinjection. *NanoBioscience, IEEE Transactions on* 7 (4): 257–266.

Wang, W., X. Liu, D. Gelinas, B. Ciruna, and Y. Sun. 2007. A fully automated robotic system for microinjection of zebrafish embryos. *PLoS One* 2 (9): e862.

Wang, W. H., X. Y. Liu, and Y. Sun. 2009. High-throughput automated injection of individual biological cells. *Automation Science and Engineering, IEEE Transactions on* 6 (2): 209–219.

Yu, S. and B. J. Nelson. 2001. Microrobotic cell injection. Paper read at IEEE International Conference on Robotics and Automation, at Seoul, Korea.

Zubir, M. N. M., B. Shirinzadeh, and Y. Tian. 2009. Development of a novel flexure-based microgripper for high precision micro-object manipulation. *Sensors & Actuators: A. Physical* 150 (2): 257–266.